

Chapter 12

Control of Cat Walking and Paw-Shake by a Multifunctional Central Pattern Generator

Brian Bondy, Alexander N. Klishko, Donald H. Edwards, Boris I. Prilutsky and Gennady Cymbalyuk

Abstract Central pattern generators (CPGs) are oscillatory neuronal networks controlling rhythmic motor behaviors such as swimming, walking, and breathing. Multifunctional CPGs are capable of producing multiple patterns of rhythmic activity with different periods. Here, we investigate whether two cat rhythmic motor behaviors, walking and paw-shaking, could be controlled by a single multifunctional CPG. To do this, we have created a parsimonious model of a half-center oscillator composed of two mutually inhibitory neurons. Two basic activity regimes coexist in this model: fast 10 Hz paw-shake regime and a slow 2 Hz walking regime. It is possible to switch from paw-shaking to walking with a short pulse of conductance in one neuron, and it is possible to switch from walking to paw-shaking with a longer pulse of excitatory conductance in both neurons. The paw-shake and walking rhythms generated by the CPG model were used as input to a neuromechanical model of the cat hindlimbs to simulate the corresponding rhythmic behaviors. Simulation results demonstrated that the multifunctional half-center locomotor CPG could produce movement mechanics and muscle activity patterns typical for cat walking or paw-shake responses if synaptic weights in selected spinal circuits were altered during each behavior. We propose that the selection of CPG regimes and spinal circuitry is triggered by sensory input from paw skin afferents.

Keywords Multifunctional multistability · Paw-shaking · Walking · Neuromechanical modeling · Cat

B. Bondy (✉) · D. H. Edwards · G. Cymbalyuk
Neuroscience Institute, Georgia State University, Petit Science Center 818,
100 Piedmont Ave SE, Atlanta, GA 30303, USA
e-mail: bbondy2@student.gsu.edu

D. H. Edwards
e-mail: dedwards@gsu.edu

G. Cymbalyuk
e-mail: gcymbalyuk@gsu.edu

A. N. Klishko · B. I. Prilutsky
School of Applied Physiology, Center for Human Movement Studies, Georgia Institute of
Technology, 555 14th Street NW, Atlanta, GA 30332, USA
e-mail: aklishko3@gatech.edu

© Springer Science+Business Media New York 2016

B. I. Prilutsky, D. H. Edwards (eds.), *Neuromechanical Modeling of Posture and Locomotion*, Springer Series in Computational Neuroscience,
DOI 10.1007/978-1-4939-3267-2_12

12.1 Introduction

Rhythmic motor behaviors, such as walking, breathing, and chewing are controlled by specialized neuronal circuits known as central pattern generators (CPGs). CPGs can produce behaviors even when deprived of sensory feedback and/or input from the brain (Marder and Calabrese 1996; Marder and Bucher 2001; Grillner 2006; McCrea and Rybak 2008). The half-center oscillator (HCO) is a ubiquitous motif in CPG connectivity. It is a simple mechanism explaining how non-rhythmic neurons can produce rhythmic output. The simplest HCO is composed of two mutually inhibitory neurons which produce a pattern of alternating single spikes or bursts of spikes (Brown 1911; Wang and Rinzel 1992; Friesen 1994; Marder and Calabrese 1996). The rhythmic activity generated by the HCO drives pattern formation in downstream interneurons which in turn activate muscles via motoneurons (McCrea and Rybak 2008).

If a CPG can produce more than one functional behavior, it is referred to as a multifunctional CPG. A multifunctional CPG can be composed of two circuits that share neurons (Getting 1989; Briggman and Kristan 2008). In both vertebrates and invertebrates, individual interneurons can contribute to multiple motor rhythms (Ritzmann et al. 1980; Lockery and Kristan 1990; Syed and Winlow 1991; Lieske et al. 2000; Popescu and Frost 2002; Berkowitz et al. 2010). There are two main mechanisms for motor program selection for multifunctional CPGs. First, *the network may be transformed* through some extrinsic process that functionally configures the CPG to produce one rhythm or another. Alternatively, *the network may demonstrate multistability*, where it is *intrinsically* capable of producing multiple rhythms and can switch between them in response to appropriate transient inputs.

Transformation can be accomplished through neuromodulation. The presence of different neuromodulators or combinations of neuromodulators can functionally reconfigure a network (by changing electrical properties of neurons and synaptic strengths) and/or change the pool of recruited neurons to produce different behaviors (Hooper and Moulins 1989; Marder et al. 1997; Crisp and Mesce 2004; Doi and Ramirez 2008). In a broad sense, to produce the correct behavior, the CPG having the correct neuromodulatory tone is *necessary and sufficient*. Tonic sensory input that does not involve neuromodulators can also transform a network by activating or suppressing certain neurons (Soffe 1997; Liao and Fetcho 2008). In this paradigm, at any given time the CPG can only produce one activity regime, and that is determined by what input it is receiving.

It is also possible that multiple behaviors could be produced by one set of neurons without external influence in a *multistable* CPG. As with any neural system, a multistable CPG would still require a certain neuromodulatory tone (Hounsgaard and Kiehn 1989; Lechner et al. 1996), but it would be able to switch between multiple activity regimes without any changes in that neuromodulatory tone. Some input would be necessary to cause a transition between regimes, but this input can be transient.

Multistability of activity regimes in neurons and networks is a common phenomenon. Bistability between spiking and silence was predicted from the original Hodgkin-Huxley model of the squid giant axon (Hodgkin and Huxley 1952; Rinzel 1978) and then demonstrated experimentally (Guttman et al. 1980). Multistability allows normally silent motoneurons to fire at high frequencies persistently after a short stimulation (Houngaard et al. 1984). In the case of motoneurons and in some other situations where bistability has been observed, slow or non-inactivating currents, such as the persistent sodium current, calcium currents, or the A-type potassium current, have been implicated as the underlying mechanism for multistability (Turrigiano et al. 1996; Hughes et al. 1999; Carlin et al. 2000; Egorov et al. 2002; Fuentealba et al. 2004). There has been a great deal of work modeling multistability of firing modes and investigating its mechanisms (Canavier et al. 1993; Butera 1998; Hahn and Durand 2001; Cymbalyuk et al. 2002; Cymbalyuk and Shilnikov 2005; Shilnikov et al. 2005; Fröhlich and Bazhenov 2006; Newman and Butera 2010; Malashchenko et al. 2011).

Models of multifunctional CPGs have been produced where multistability between fast and slow rhythms or phase relationships is the result of slow variables in synaptic dynamics (Bose and Kunec 2001; Manor and Nadim 2001; Chuan et al. 2004). The possibility that multistability in a CPG could arise from cellular dynamics has not been explored. It is not clear whether cellular dynamics can provide multistability in a network of neurons. Cellular dynamics are an alternative mechanism for multistability in a CPG.

Specifically, we investigated whether a pair of well-studied cat behaviors, walking and paw-shaking, could be produced by a single HCO. Both behaviors involve many of the same muscles, and can be elicited in a spinalized cat, even when motion-dependent sensory feedback has been removed, indicating both regimes are produced to a large extent by CPG (Carter and Smith 1986; Koshland and Smith 1989; Pearson and Rossignol 1991). The paw-shake response is initiated when a stimulus, such as an adhesive tape or water, becomes stuck to cat's paw. It consists of rapid (about 10 Hz) rhythmic movements of the paw. Walking, commonly referred to as stepping or locomotion, is a slower regime, usually around 1–2 Hz.

12.2 Model of Multifunctional Central Pattern Generator

The neurons were modeled using the Hodgkin and Huxley formalism (Hodgkin and Huxley 1952). Each neuron contains six ionic currents: a fast sodium current (I_{NaF}), a slow sodium current (I_{NaS}), a potassium current (I_K), a slow calcium current (I_{CaS}), a synaptic current (I_{syn}), and a leak current (I_{leak}). Parameters for I_{Na} , I_K , and I_{leak} were taken from (Rybak et al. 2006). Conductances were modified to make the model produce paw-shaking-like and walking-like bursting activities. Additionally, a seventh current, I_{Mod} , which could be expressed as either I_I or I_E (inhibitory or excitatory modulatory current) based on the equilibrium potential, could be turned on and off in a time dependent and cell specific manner. There are a total of seven

state variables in each cell: voltage, inactivation of I_{NaF} , I_{NaS} , and I_{CaS} , activation of I_{NaS} , I_K , I_{CaS} and I_{Syn} . Activations of I_{NaF} , I_{Mod} , and I_{Leak} are considered instantaneous and are simply functions of the membrane potential. The membrane potential is governed by the current conservation equation:

$$CV' = -[I_{NaF} + I_{NaS} + I_K + I_{CaS} + I_h + I_{Mod} + I_{leak} + I_{syn}]$$

$I_{NaF} = \bar{g}_{NaF} m_{NaF,\infty}^3 h_{NaF} [V - E_{Na}]$	$E_{Na} = 65 \text{ mV}$	$\bar{g}_{NaF} = 40 \text{ nS}$
$I_{NaS} = \bar{g}_{NaS} m_{NaS} h_{NaS} [V - E_{Na}]$		$\bar{g}_{NaS} = 3.9 \text{ nS}$
$I_K = \bar{g}_K m_K^4 [V - E_K]$	$E_K = -70 \text{ mV}$	$\bar{g}_K = 40 \text{ nS}$
$I_{CaS} = \bar{g}_{CaS} m_{CaS}^3 h_{CaS} [V - E_{Ca}]$	$E_{Ca} = 160 \text{ mV}$	$\bar{g}_{CaS} = 12 \text{ nS}$
$I_{Mod} = \bar{g}_{Mod} [V - E_{Mod}]$	$E_I = -75 \text{ mV}$	$E_E = 70 \text{ mV}$
$I_{leak} = \bar{g}_{leak} [V - E_{leak}]$	$E_{leak} = -54 \text{ mV}$	$\bar{g}_{leak} = 3 \text{ nS}$
$I_{Syn} = \bar{g}_{Syn} m_{Syn} [V_{pre} - E_{Syn}]$	$E_{Syn} = -75 \text{ mV}$	$\bar{g}_{Syn} = 5.5 \text{ nS}$

$$m_{NaF,\infty} = \frac{1}{1 + \exp\left(\frac{V + 18.5}{-7.8}\right)},$$

where \bar{g}_x and E_x are the maximal conductance and reversal potential for current I_x , respectively.

Membrane potential of the neuron in the above equations is indicated by V while V_{pre} (seen in last, synapse equation) indicates membrane potential of the other neuron. m refers to activation variables, h refers to inactivation variables. All equations are identical in both neurons except with respect to I_{Mod} , which has a term that can make it active in one, both, or neither neurons. The conductance of I_{Mod} was zero except during specified time interval. When I_{Mod} is excitatory (I_E), $E_{Mod} = E_E = 70 \text{ mV}$. When I_{Mod} is inhibitory (I_I), $E_{Mod} = E_I = -75 \text{ mV}$. In the text, I_{Mod} will be referred to as either I_E or I_I , and its conductance as either g_E or g_I . All voltages are in mV, all conductances are in nS, and all currents are in pA. In the CPG model, time is in seconds, whereas in the text, time is in milliseconds. The parameters were not changed at any point during simulations presented in this article.

12.2.1 Computer Simulations

The differential equations were solved in Matlab (The MathWorks, Inc., Natick, MA, USA) using the ode15s differential equation solver. An absolute and relative integration tolerance of $1 \cdot 10^{-10}$ was used, as well as an initial step of 0.0001 s and a max step of 0.005 s. A time step size of at least 0.0001 s was used for simulations that were part of any analysis. Sections of simulations where the neurons had not reached a steady state were discarded.

Burst duration is calculated as the time between the first and last spike of a burst. Inter-burst interval is the time between the last spike of a burst and first spike of the next burst, period is the sum of inter-burst interval and burst duration, and duty cycle is burst duration divided by period. Frequency is the inverse of the inter-spike interval, and mean frequency is the mean frequency of all the spikes in a burst and is calculated as the number of spikes per burst divided by burst duration. Maximal frequency and minimum frequency were calculated as the inverse of the smallest and largest inter-spike intervals in a burst, respectively. Coefficient of variation is the standard deviation as a percent of the sample mean. Charge was calculated as the integral of current with respect to time for each burst period.

12.2.2 Simulation Results

12.2.2.1 Model Activity

The developed half-center oscillator model can exhibit walking-like and paw shake-like regimes of rhythmic activity. This HCO contains two mutually inhibitory model neurons that are not endogenously bursting. When coupled, the neurons burst in antiphase.

The isolated neuron ($\bar{g}_{syn} = 0 \text{ nS}$) spikes tonically (Fig. 12.1). During baseline spiking activity, I_{CaS} is close to zero (I_{CaS} trace in Fig. 12.1, before conductance pulse) because I_{CaS} is almost completely inactivated; the inactivation variable for I_{CaS} (h_{CaS}) was never higher than $5 \cdot 10^{-6}$. The rhythmic spiking activity is predominantly driven by I_{NaS} . However, if the neuron is strongly hyperpolarized by an inhibitory current, I_I (Fig. 12.1, $g_I = 1 \text{ nS}$, $E_I = -75 \text{ mV}$), I_{CaS} and I_{NaS} will deactivate and produce transient rebound bursting. The conductance pulse (100 ms duration) produced a rebound burst that is similar to the bursts in the walking regime (Fig. 12.2b). The first burst has duration of 290 ms, a maximal frequency of 641 Hz, a minimum frequency of 51 Hz, and 82 spikes per burst (Fig. 12.1). Over the course of subsequent bursts, burst duration, spikes per burst, and spike frequency all decrease along with h_{CaS} until the neuron returns to tonic spiking.

We developed an HCO based on the rebound bursting properties seen in the isolated neuron. The introduction of inhibitory synaptic coupling with the same equilibrium potential (-75 mV) as I_p and a conductance of 5.5 nS results in antiphase bursting. The synapse is activated during spiking, and higher frequency spiking in the postsynaptic neuron results in increased summation of I_{syn} in the postsynaptic neuron. The model exhibited two basic modes of activity, which we refer to as paw-shake and walking (Fig. 12.2). These regimes differ both in burst characteristics and dynamics of bursting. Formally, the model exhibits two paw-shake regimes which are very similar in every measure. They differ in number of spikes per burst; one has 5 spikes per burst and the other has 6 spikes per burst. Here, we refer to them as paw-shake regime. Paw-shake is a fast regime. It has a period of about 100 ms and a duty cycle of 32% (Fig. 12.2a). The bursts display a maximum spike frequency of

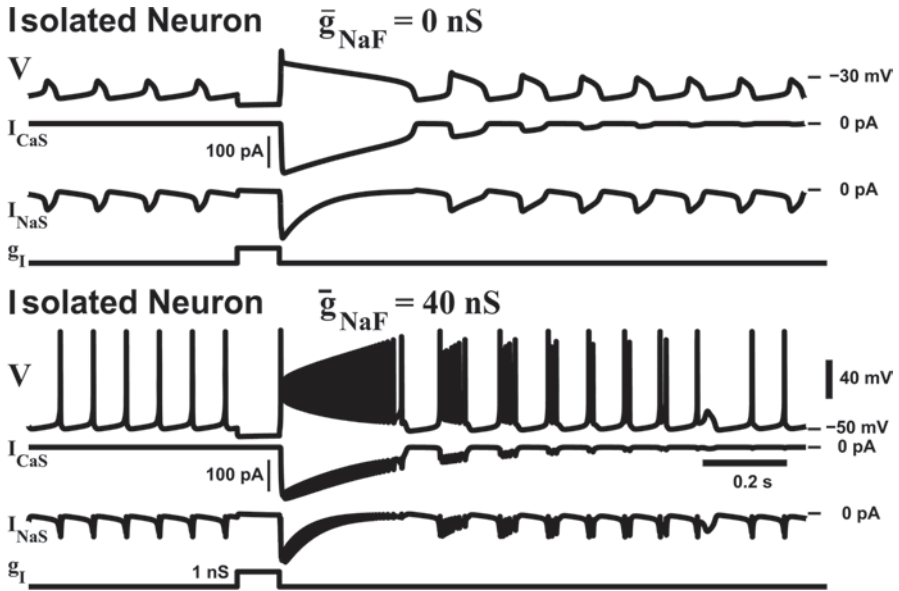


Fig. 12.1 Activity in an isolated model neuron. Traces show spontaneous activity of the isolated neuron and response to a pulse of inhibitory conductance (g_I). V is membrane potential of the isolated neuron. The neuron is isolated by setting all of the conductances in Neuron 2 to zero. The conductance for the inhibitory modulatory current (I_I) is shown as the bottom trace. It is zero, except for a 100 ms window, where it is equal to 1 nS. I_I has an equilibrium potential of -75 mV

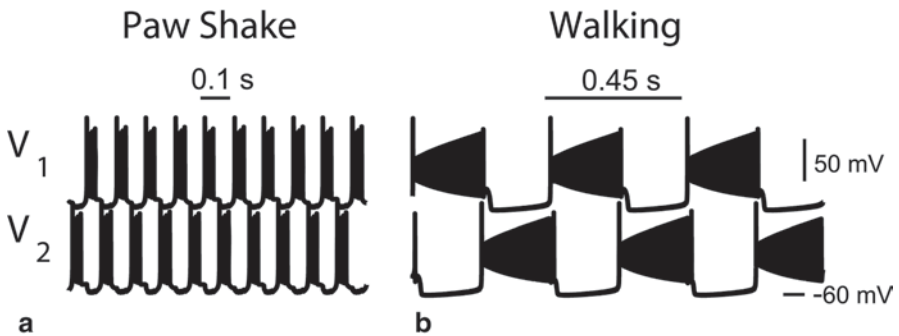


Fig. 12.2 Coexistence of paw shake and walking regimes in the model. All simulations were given at least 1000 s to reach steady state

196 Hz at the beginning of a burst, a minimum frequency of 100 Hz at the end of a burst, and a mean frequency of 152 Hz.

The walking regime is the slowest of the exhibited regimes. It has a period of about 450 ms and a duty cycle of 52%. The bursts display a maximum spike frequency of 620 Hz near the beginning of a burst, a minimum frequency of 100 Hz at the end of a burst, and a mean frequency of 399 Hz (Fig. 12.2b).

12.2.2.2 Comparisons Between Walking and Paw-Shake Regimes

There are several major differences between the regimes. First is that there are very different levels of I_{CaS} contribution. The peak value for I_{CaS} in each burst is 40 times larger in the walking regime compared to paw-shake. Second is the magnitude of I_{Syn} . The mean value for I_{Syn} in each burst is twice as larger in the walking regime compared to paw-shake. Finally, there is a large difference in maximal frequency between regimes. Paw-shake has a peak frequency of 196 Hz and walking has a peak frequency of 620 Hz. These three measures are interdependent. Increases in I_{CaS} increases spike frequency, which in turn increases I_{Syn} through summation of inhibitory postsynaptic potentials. All of this worked to change the period of bursting activity.

There are also many similarities between these bursting regimes. Burst initiation in all regimes is the result of I_{NaS} activation/deinactivation. Likewise, burst termination is the result of inactivation of the slow inward currents. In the case of walking, escape of the postsynaptic neuron from inhibition also plays a role in burst termination, but this escape occurs when the presynaptic neuron's spike frequency falls close to 100 Hz.

12.2.2.3 Switching Regimes

An important feature of multistable systems such as the developed HCO is that transient perturbations can cause a switch between regimes. Studying how our HCO model switches between the walking and paw-shake regimes can help us make testable predictions about these behaviors in the cat. In a CPG, perturbations can come from sensory neurons or brain areas. Theoretically, an object attached to a cat's paw could activate cutaneous afferents that synapse with interneurons comprising CPG circuitries and induce a switch between walking and paw-shake regimes. We used pulses of conductance (either excitatory or inhibitory) to mimic such perturbations with the goal of studying CPG transitions between walking and paw-shake regimes.

Switch from Walking to Paw-Shake Switching from walking to paw-shake CPG regimes requires inactivating I_{CaS} . This is possible by introducing an excitatory modulatory current I_E with an equilibrium potential of +70 mV. The conductance (g_E) was set so that both neurons would be spiking during stimulation (Fig. 12.3, during g_E pulse). As long as the neurons spiking tonically, I_{CaS} will inactivate (as in Fig. 12.1). The threshold (in terms of the values for the inactivation variables) for switching between regimes is closer to paw-shake than walking. This means I_{CaS} must be almost completely inactivated for the model to switch to paw-shake. Therefore, the length of stimulation time (pulse duration) depends on the time constant of inactivation for I_{CaS} , and thus a long pulse duration is needed for the switch from walking to paw-shake.

Switch from Paw-Shake to Walking A brief hyperpolarization to an isolated model neuron can cause a substantial deinactivation of I_{CaS} and a large rebound burst

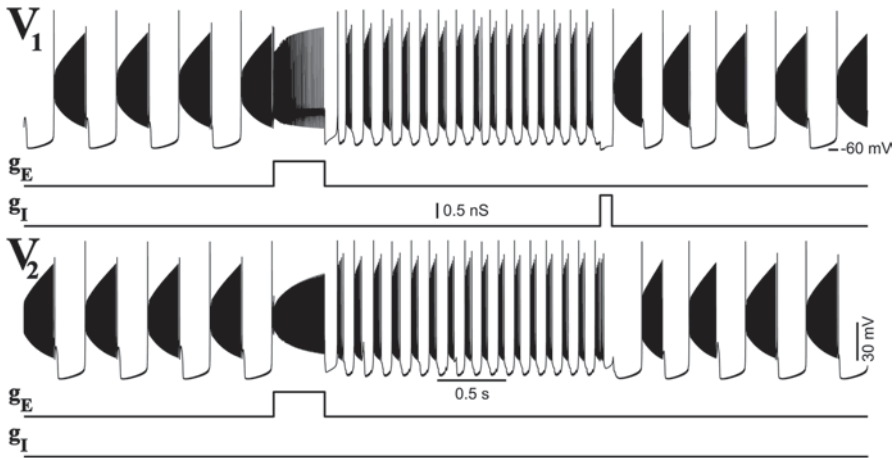


Fig. 12.3 Switching back and forth between rhythms. V_1 and V_2 represent Neuron 1 and Neuron 2, respectively. The neurons begin in the walking rhythm. An optimally timed pulse of excitatory conductance (g_E for I_E ; $g_E = 0.8$ nS, I_E equilibrium potential = 70 mV, pulse duration = 370 ms) delivered to both neurons causes a switch to paw-shaking. During the pulse, cells are not firing in antiphase. A pulse of inhibitory conductance (g_I for I_p ; $g_I = 0.85$ nS, I_I equilibrium potential = -75 mV, pulse duration = 90 ms) is delivered to neuron 1 only, causing a rebound burst and a switch back to walking

(Fig. 12.1). This is equally true in the coupled neurons. A brief hyperpolarization of sufficient magnitude could produce a rebound burst just as long as a burst in the walking regime (Fig. 12.1). In the isolated neuron, the resulting bursting would be transient. However, if a hyperpolarization was given to a neuron in the HCO while in the paw-shake rhythm, it could cause a switch to the walking regime.

Delivering a hyperpolarizing pulse to a neuron in the HCO while in paw-shake can have two outcomes, depending on the strength of the hyperpolarization. A hyperpolarization will still produce a rebound burst with a longer period and a higher spike frequency than a normal paw-shake burst. The rebound burst will inhibit the non-stimulated neuron more strongly and deactivate I_{CaS} . If the original hyperpolarization is strong enough, each subsequent burst will have a longer period and higher spike frequency until the HCO reaches the steady state walking rhythm. If the original hyperpolarization is too small, each subsequent burst will be smaller, until the HCO returns to the steady state paw-shake regime.

External inhibitory command signal was simulated using an inhibitory modulatory current I_p with an equilibrium potential of -75 mV. By having I_p active in one neuron for as little as 45 ms it was possible to induce a switch from paw-shake to walking. Longer pulses were needed for a rapid transition (Fig. 12.3, 90 ms inhibitory conductance pulse), although shorter pulse durations could have the same effect if g_I was larger. Depending on the pulse duration and the conductance of I_p , the transition could occur very rapidly, with the walking regime reaching its normal period within two cycles as in Fig. 12.3. Very strong inhibition (higher conductance or longer pulse duration) causes a seizure-like rebound burst followed by normal

walking activity. Phase of stimulation had little effect on transitions, except at very low values of g_f (data not shown).

A brief inhibition of one neuron, as in Fig. 12.3, is the fastest way to produce a transition. It is possible to produce a switch with inhibitory pulses to both neurons. These transitions always take longer since both neurons will burst at the same time upon release of the inhibition. Persistent inhibition of sufficient strength will also cause a switch to walking (after several seconds) or actually make the paw-shake regime disappear entirely (data not shown).

12.3 Neuromechanical Simulations of Walking and Paw-Shake

The previous sections described a multifunctional CPG that can generate fast paw shake-like and slow walking-like rhythmic reciprocal activity depending on parameters of the HCO and input to the system in the form of a conductance pulse. In the following sections, we present preliminary results of neuromechanical simulations of cat walking and paw-shake developed using the AnimatLab software for neuromechanical simulations (Cofer et al. 2010). In these simulations, the musculoskeletal model of the hindlimb is controlled by a CPG that consists of a half-center oscillator (HCO) generating rhythmic activity with frequency of either 2 or 10 Hz. Motoneurons activating 12 flexor and extensor muscles in each hindlimb (Fig. 12.4) receive excitatory input from the corresponding half-center oscillator and also excitatory and inhibitory inputs from muscle length- and force-sensitive afferents (Fig. 12.5).

The goal of these neuromechanical simulations was to examine if a single multifunctional HCO could reproduce two very different rhythmic behaviors, walking and paw-shake. These behaviors differ not only in the cycle duration but also in movement mechanics and patterns of muscle activity (Smith et al. 1985; Smith and Zernicke 1987; Prilutsky et al. 2004, 2009; Klishko et al. 2012; Mehta and Prilutsky 2014). In particular, during walking, flexor and extensor muscles are activated reciprocally (Markin et al. 2012), whereas during paw-shake response, anterior and posterior muscles, rather than flexors and extensors, appear to demonstrate reciprocal activation (Smith et al. 1985; Pratt et al. 1991; Klishko et al. 2012).

12.3.1 Musculoskeletal Model of Cat Hindlimb

A cat hindlimb model was assembled in the Body Plan Editor of AnimatLab as a system of 5 rigid segments representing the pelvis, thigh, shank, tarsals and toes. Inertial properties of each segment, i.e., segment mass, position of the center of segment mass, and moment of inertia with respect to the frontal axis through the center mass of the segment, were computed from the measured cat mass and segment

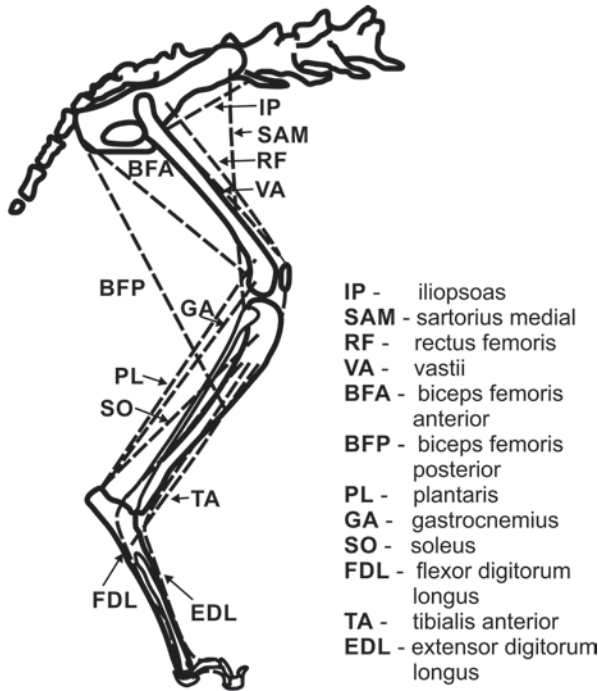


Fig. 12.4 Musculoskeletal model of the cat hindlimb (model of the second hindlimb is identical). The hindlimb skeleton is represented by a system of 5 rigid segments (pelvis, thigh, shank, tarsals and toes) interconnected by frictionless hinge articulations (hip, knee, ankle and metatarsophalangeal, MTP, joints). The model is actuated by 12 Hill-type muscles that include iliopsoas (*IP*, hip flexor), sartorius medial (*SAM*, hip and knee flexor), rectus femoris (*RF*, hip flexor and knee extensor), BFA (hip extensor), BFP (hip extensor and knee flexor), vastii (knee extensor), tibialis anterior (*TA*, ankle flexor), extensor digitorum longus (*EDL*, ankle and MTP flexor), plantaris (*PL*, knee flexor and ankle extensor), gastrocnemius (*GA*, knee flexor and ankle extensor), soleus (*SO*, ankle extensor), flexor digitorum longus (*FDL*, ankle and MTP extensor)

length using the regression equations (Hoy and Zernicke 1985). The hindlimb segments were interconnected by frictionless hinge joints. The hindlimb skeleton was actuated by 12 muscles (Fig. 12.4). Points of each muscle origin and attachment were estimated based on the geometric model of a cat hindlimb (Goslow et al. 1973). Muscle paths were modeled as sets of straight lines connecting selected via points so that the moment arms of each muscle at joints it crosses corresponded roughly to the values reported in the literature (Boyd and Ronsky 1998; MacFadden and Brown 2007, 2010). Muscles and muscle spindles (see below) were represented by Hill-type models consisting of an elastic component (tendon) attached in series with the parallel combination of a parallel elastic component (passive connective tissues surrounding muscle fibers and compartments) and a contractile component (the cross-bridges). The physiological properties of the contractile component were described in the model by the muscle membrane voltage-contractile force curve, isometric force-length curve, force-velocity relationship, the optimum muscle length

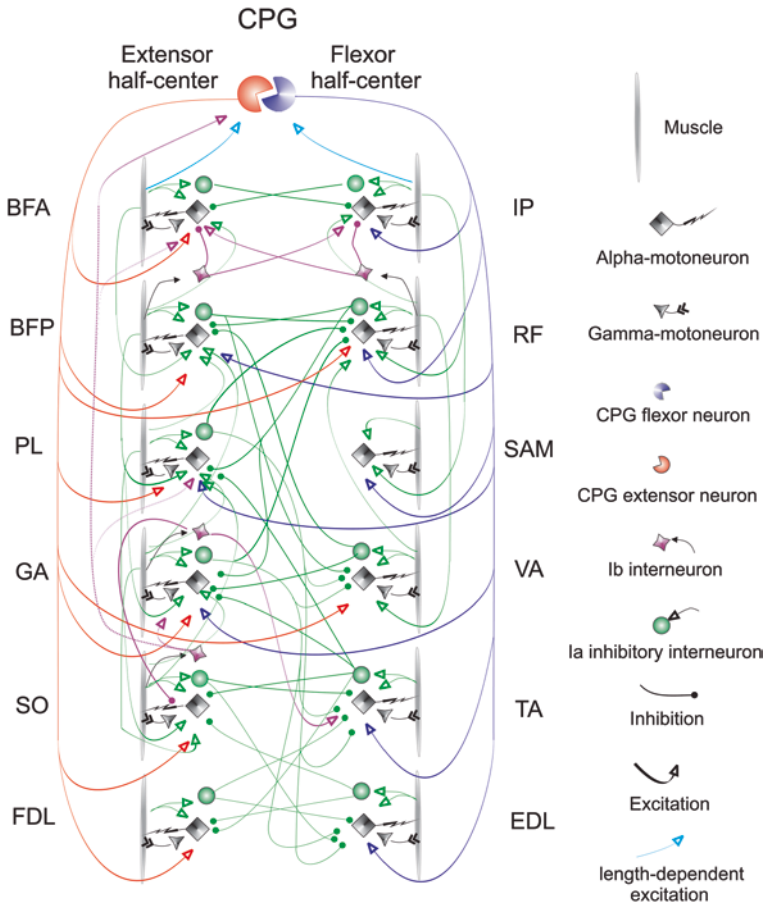


Fig. 12.5 Neural control model of cat hindlimb. The model consists of a central pattern generator (CPG) and basic reflex pathways. CPG generates symmetric flexor and extensor rhythmic activity with a frequency of either 10 Hz (paw-shake rhythm) or 2 Hz (locomotion rhythm). The extensor and flexor half-centers provide excitatory input to motoneurons of one-joint extensors and flexors, respectively. Motoneurons of two-joint muscles may receive excitations from both half-centers in flexor and extensor phases. Reflex pathways include stretch reflex with reciprocal inhibition that is mediated by Ia spindle afferents and Ia-inhibitory interneurons, respectively; force-dependent inhibition and excitation from two-joint muscles to one-joint synergists and one-joint antagonists, respectively; force-dependent excitation of the CPG extensor half-center from SO motoneuron during the extensor phase of the CPG; and length-dependent excitation from hip flexor and extensor muscle to the CPG flexor- and extensor-half center, respectively (see text for more details). For muscle abbreviations see Fig. 12.4

and maximum force (Table 12.1; see also Cofer et al. 2010). Each muscle in the model had sensors of length (the spindle) and force (the Golgi tendon organ). The spindle force was generated in response to gamma motoneuron input and stretch of the muscle contractile component. Spindle force generated depolarizing membrane current in the spindle neuron that fired when the membrane potential exceeded the

Table 12.1 Parameters of the muscle model

Muscle	B (Ns/m)	K_{pe} (N/m)	K_{se} (kN/m)	F_{max} (N)	PE_{len} (%)	L_{rest} (cm)	L_{width} (cm)
IP	30.9	385	13.351	150	55	7.0	5.0
BFA	8.2	227	6.464	120	36	12.0	5.0
BFP	40.0	806	27.837	250	56	11.5	5.5
SAM	3.3	100	2.357	20	91	12.1	5.5
RF	25.0	642	15.844	122	20	11.1	3.0
VA	20.0	3125	34.014	250	27	11.1	8.0
PL	18.4	370	11.905	200	90	12.1	4.2
GA	18.4	370	11.905	200	23	12.5	4.2
SO	2.0	36	1.667	21	58	9.1	12.0
TA	10.1	191	4.643	65	57	10.1	2.8
EDL	10.0	105	2.484	40	35	11.7	1.7
FDL	20.0	433	7.738	130	17	12.1	2.0

Muscle abbreviations are the same as in Fig. 12.4

B is viscosity of the linear force-velocity relationship of the muscle contractile component, K_{pe} is stiffness of the parallel elastic component, K_{se} is stiffness of the serial elastic component, F_{max} is maximum muscle isometric force at optimal (resting) length of the contractile component, PE_{len} is percentage of the parallel elastic component resting (optimal) length in the total muscle-tendon unit length, L_{rest} is resting (optimal) length of the muscle, L_{width} is the muscle length range for active force production in the isometric force (F_L)-length (L) relationship: $F_L = 1 - (L - L_{rest} / L_{width})^2$. For details on the AnimatLab muscle model see (Cofer et al. 2010)

threshold. Tendon Golgi organ sensory signal was proportional to force produced by the muscle.

For simulations of walking, each hindlimb was connected to the trunk, which could move without friction along an elastic string (stiffness coefficient 5 MN/m) thus providing partial weight support to substitute support from the forelimbs that were not included in the model.

12.3.2 Neural Control Model

A model of the neural control circuitry activating hindlimb muscles during walking and paw-shake was developed in the Behavior Editor of AnimatLab. The HCO was modelled by two spiking integrate-and-fire single compartment neurons mutually inhibiting each other via hyperpolarizing IPSP. Output of extensor and flexor half-centers activated motoneurons represented by non-spiking voltage- and time-dependent ionic conductance neurons (Vogels et al. 2005) via the same non-spiking interneurons that transformed spiking trains from the HCO into integrated membrane potential. The output of a single motoneuron represented an integrated output (membrane voltage) of a motoneuronal pool activating a single muscle. Motoneurons activated corresponding muscles that produced force in accordance with the stimulus (membrane voltage)-force curve (Cofer et al. 2010). Each motoneuron

received excitatory inputs from the HCO and excitatory and inhibitory inputs from various reflex pathways (Table 12.2).

All motoneurons received length- and velocity-dependent monosynaptic excitatory inputs from the Ia spindle afferents of anatomical synergists (Fig. 12.5, open arrow heads; Table 12.2). Reciprocal inhibition among anatomical antagonists (e.g., soleus and tibialis anterior, vastii and gastrocnemius) was mediated via Ia inhibitory interneurons (Fig. 12.5, green circles; Table 12.2; Feldman and Orlovsky 1975; Geertsen et al. 2011). Excitation of one-joint antagonists and inhibition of one-joint agonists from two-joint muscles (e.g., excitation of tibialis anterior and inhibition of soleus from gastrocnemius) were mediated by Golgi tendon force-dependent pathways (Fig. 12.5; Table 12.2; Laporte and Lloyd 1952; Eccles et al. 1957; Nichols 1999, see also Chap. 3 by Nichols et al. 2015). The neural control model also incorporated afferent pathways that regulated the operation of the CPG during locomotion. Excitatory length-dependent afferent input from a hip flexor iliopsoas to the flexor half-center triggered transition from extensor to flexor phase of rhythmic activity, whereas excitatory length-dependent afferent signals from hip extensor biceps femoris anterior to the extensor half-center triggered transition from flexor to extensor phase (Fig. 12.5; Table 12.3; Kriellaars et al. 1994; Hiebert et al. 1996; McVea et al. 2005). A force-dependent afferent input during the extensor phase of the cycle from ankle extensor soleus to the extensor half-center and to extensor motoneurons enhanced activity of hindlimb extensors (Fig. 12.5; Table 12.3; Conway et al. 1987; McCrea 2001; Pearson 2008).

12.3.3 *Neuromechanical Simulations*

12.3.3.1 **Paw-Shake**

In order to qualitatively reproduce patterns of muscle activity typical for paw-shake, i.e. alternating reciprocal activity of anterior and posterior hindlimb muscles (Smith et al. 1985; Pratt et al. 1991; Klishko et al. 2012), as opposed to alternating activity of flexor and extensor muscles observed during locomotion (Grillner 1981; Rossignol 2006; Markin et al. 2012), gains of afferent excitatory and inhibitory feedback actions on motoneurons were modified. Specifically, autogenic (from a muscle to its own motoneuron) and heterogenic (from a muscle to synergist motoneurons) Ia afferent feedback gains were increased (Table 12.2) given the very high firing rates of Ia afferents from various cat muscles during paw-shake (Prochazka et al. 1989). In addition, the excitatory force (Ib)-dependent input from ankle extensor soleus to the extensor half-center oscillator and extensor motoneurons during the extensor phase was removed to make the extensor and flexor phases equal in duration (Table 12.3).

Before each simulation, the initial hindlimb position approximately corresponding to that observed in experiments (see below) was set by tonic activity of IP and BFP motoneurons and maintained for 2 s. In this initial position hip, knee, ankle and

Table 12.2 Weight coefficients of neural pathways to motoneurons during walking

MN or muscle	CPG _F (μS)	CPG _E (μS)	I_{a_0} (kHz/m)	C_{lar^+} (nAs)/ D_{lar^+} (nA)	C_{lar^-} (nAs)/ D_{lar^-} (nA)	C_{ib^+} (nAs)/ D_{ib^+} (nA)	C_{ib^-} (nAs)/ D_{ib^-} (nA)
IP	0.1	–	100	IP(0.1/0) RF(0.1/0)	BFA(0.3/0)	BFP(0.001/0)	RF(0.001/0)
BFA	–	0.002	50	BFA(0.1/0) BFP(0.08/0)	IP(0.1/0)	RF(0.001/0)	BFP(0.005/0)
BFP	0.003	0.01	30	BFP(0.05/0) GA(0.1/0) BFA(0.1/0)	VA(0.2/0) RF(0.1/0)		
SAM	0.3	0	30	SAM(0.2/0) IP(0.1/0)			
RF	0.03	0.001	100	RF(0.4/0) IP(0.1/0) VA(0.2/0)	BFP(0.5/0) GA(0.4/–20) PL(0.1/0)		
VA	–	0.003	40	VA(0.2/0) RF(0.1/0)	GA(0.1/0) PL(0.1/0) BFP(0.05)	BFP(0.001/0)	RF(0.001/0)
PL	0.001	0.05	30	PL(0.1/–8) BFP(0.05/0)	RF(0.2/0) TA(0.1/0)		
GA	0.001	0.05	30	GA(0.2/0) BFP(0.05/0)	RF(0.2/0) TA(0.1/0)		
SO	–	0.1	40	SO(0.1/0) GA(0.01/0) PL(0.01/0)	EDL(0.1/0)		GA(0.01/0)
TA	0.1	–	50	TA(0.2/–15)	GA(0.1/0) PL(0.1/0) SO(0.1/0) FDL(0.05/0)	GA(0.002/0)	

Table 12.2 (continued)

MN or muscle	CPG _F (μS)	CPG _E (μS)	I_{a_0} (kHz/m)	C_{Ia+} (nAs)/ D_{Ia+} (nA)	C_{Ia-} (nAs)/ D_{Ia-} (nA)	C_{Ib+} (nAs)/ D_{Ib+} (nA)	C_{Ib-} (nAs)/ D_{Ib-} (nA)
EDL	0.02	–	40	EDL(0.1/–10)	GA(0.1/–15) PL(0.1/–15) SO(0.3/–10) FDL(0.1/–10)		
FDL	–	0.05	40	FDL(0.1/–10)	TA(0.5/–55) EDL(0.1/–10)		

MN is motoneuron, *MN* abbreviations are the same as muscle abbreviations in Fig. 12.4. CPG_F and CPG_E are conductances of nicotinic acetylcholine (ACh) synapses mediating excitatory inputs to motoneurons from the flexor and extensor CPG half-centers, respectively; I_{a_0} is the firing rate constant of the Ia stretch receptor; C_{Ia+} and D_{Ia+} are constants in the relationship describing the autogenic or heterogenic motoneuron excitatory input current (I , nA) as a function of the Ia afferent firing rate (R, Hz): $I = C_{Ia+}R + D_{Ia+}$; C_{Ia-} and D_{Ia-} are constants in the relationship describing the motoneuron inhibitory input current (I , nA) as a function of the Ia inhibitory interneuron firing rate (R, Hz): $I = C_{Ia-}R + D_{Ia-}$; C_{Ib+} and D_{Ib+} are constants in the relationship between the motoneuron excitatory input current (I , nA) as a function of the Ib afferent firing rate (R, Hz): $I = C_{Ib+}R + D_{Ib+}$; C_{Ib-} and D_{Ib-} are constants in the relationship between the motoneuron inhibitory input current (I , nA) as a function of the Ib afferent firing rate (R, Hz): $I = C_{Ib-}R + D_{Ib-}$. During walking, IP gamma-motoneuron was stimulated with 32 nA input current; all other motoneurons did not have gamma-motoneuron input

The following changes in the weight coefficients were made to simulate paw-shake. To set the initial hindlimb posture before paw-shake, IP and BFP motoneurons were stimulated with input current 17 and 10 nA, respectively. To increase sensitivity of spindle Ia afferents, the corresponding gamma-motoneurons received the following input currents: IP, 30 nA; BFA, 29.8 nA; BFP, 32 nA; RF, 22 nA; SAM, 40 nA; GA, 32 nA; PL, 30 nA; VA, 24 nA; TA, 26 nA; SO, 20 nA; EDL, 24 nA; FDL, 20 nA. In addition, constants C_{Ia+}/D_{Ia+} were changed for the following Ia autogenic and heterogenic inputs to motoneurons: BFA Ia to BFA MN, 0.3/0; RF Ia to RF MN, 0.4/–30; VA Ia to RF MN, 0.1/–4; GA Ia to GA MN, 0.2/–15.

AnimatLab models of neurons and synapses and their properties are described in (Cofer et al. 2010)

Table 12.3 Weight coefficients of afferent pathways to CPG flexor and extensor half-centers during walking

Afferent pathway	C_{F+} (nAs)	C_{E+} (nAs)
SO Ib	–	0.3
IP Ia	0.01	–
BFA Ia	–	0.01
IP II	0.01	–
BFA II	–	0.01

Muscle abbreviations are the same as in Fig. 12.4. C_{F+} and D_{E+} are constants in the relationship describing the afferent excitatory input current (I , nA) to the CPG flexor and extensor half-center as a function of the afferent firing rate (R , Hz): $I = C_{F+}R$ or $I = C_{E+}R$. Additional excitatory input from SO Ib afferents during the extensor phase of walking was also provided to hindlimb extensor motoneurons with the following weight constants: $C_{BFA+} = 0.15$, $C_{RF+} = 0.08$, $C_{VA+} = 0.1$, $C_{PL+} = 0.03$, $C_{GA+} = 0.1$, and $C_{SO+} = 0.01$

In paw-shake simulations, all weight coefficients of the Ib excitatory pathways operating during the extensor phase to the CPG extensor half-center and extensor motoneurons were set to zero

metatarsophalangeal joint angles were 105°, 49°, 93°, and 178°, respectively. Paw-shaking was generated by fast regime of the HCO (see Sect. 12.2.) that produced alternating bursting activity in the flexor and extensor half-centers with frequency of 10 Hz. Patterns of computed muscle forces were compared to low-pass filtered activity of cat hindlimb muscles that were recorded in cats with chronically implanted intramuscular EMG electrodes (Figs. 12.6 and 12.7).

Detailed description of surgical implantations and experiments can be found elsewhere (Gregor et al. 2006; Prilutsky et al. 2011; Mehta and Prilutsky 2014). Briefly, all surgical and experimental procedures were in agreement with US Public Health Service Policy on Humane Care and Use of Laboratory Animals and approved by the Institutional Animal Care and Use Committee of Georgia Institute of Technology. Surgery for implantation of EMG electrodes was performed under general anesthesia and aseptic conditions. Vital physiological parameters (temperature, respiration, heart rate and blood pressure) were monitored throughout the surgery. Pairs of teflon-insulated multi-stranded stainless steel fine wires (CW5402; Cooner Wire, Chatsworth, CA, USA) attached to a multi-pin Amphenol connector fixed on the skull were implanted in selected hindlimb muscles (majority of muscles shown in Fig. 12.4). After surgery, the animal received pain medication and antibiotics as needed and recovered for 2 weeks.

Prior to implantation surgery cats were trained to walk on a Plexiglas enclosed walkway with embedded small force plates (Bertec Corporation, Columbus OH, USA) using positive reinforcement with food. Reflective markers placed on major hindlimb joints with double sided adhesive tape and a 6-camera motion capture system Vicon (Oxford, UK) were used to record kinematics of walking and paw-shake. Paw-shake responses were evoked by attaching a piece of adhesive tape to the paw pad on the right hindlimb. EMG activity, kinematics and ground reaction forces during paw-shake and walking were recorded synchronously at a sampling rate of 3000, 120, and 360 Hz, respectively. Kinematic and ground reaction force measurements were used to identify stance and swing phases during walking and cycles during paw-shakes.

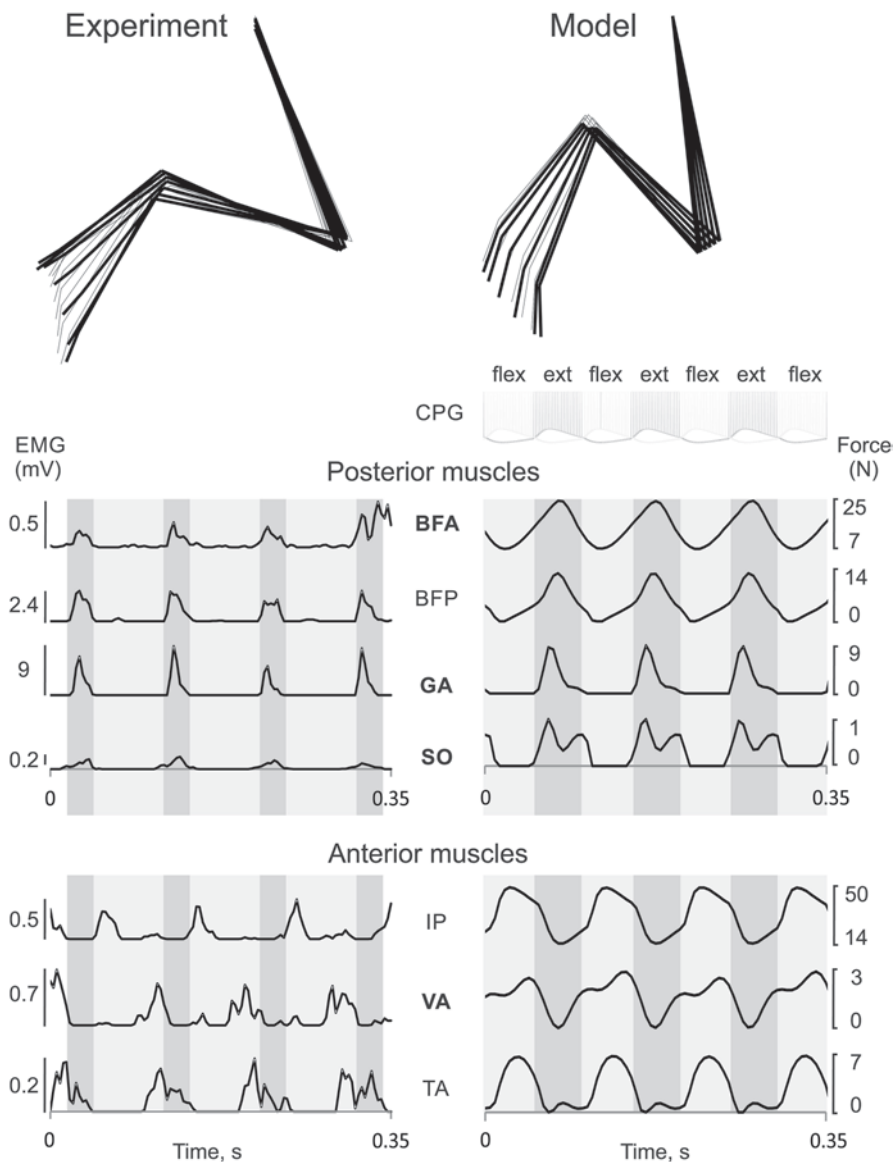


Fig. 12.6 Experimental low-pass filtered EMG patterns of hindlimb muscles during paw-shake (mean cycle duration 0.100 s; *left* panels) and patterns of muscle forces computed in computer simulations (mean cycle duration 0.088 s; *right* panels). For muscle abbreviations see Fig. 12.4; abbreviations of extensor muscles are indicated by bold font. *Top* panels show stick-diagrams of the hindlimb during a recorded and simulated paw-shake cycle; *gray lines* indicate downward foot movement in one half-cycle, *black lines* correspond to upward foot movement in the next half-cycle. Second panel in the right column demonstrates simulated bursting activity of the flexor (*light lines*) and extensor (*darker lines*) half-centers of the CPG. Next panels show experimental low-pass filtered EMG (*left*) and simulated force patterns (*right*) of selected posterior muscles. Their activity and force production occur mostly during the extensor phase of the CPG activity (*dark gray rectangles*). The *bottom* panels demonstrate experimental low-pass filtered EMG (*left*) and simulated force patterns (*right*) of selected anterior muscles. Their activity and force production occur mostly during the flexor phase of the CPG activity (*light gray rectangles*). Experimental results are from one representative cat

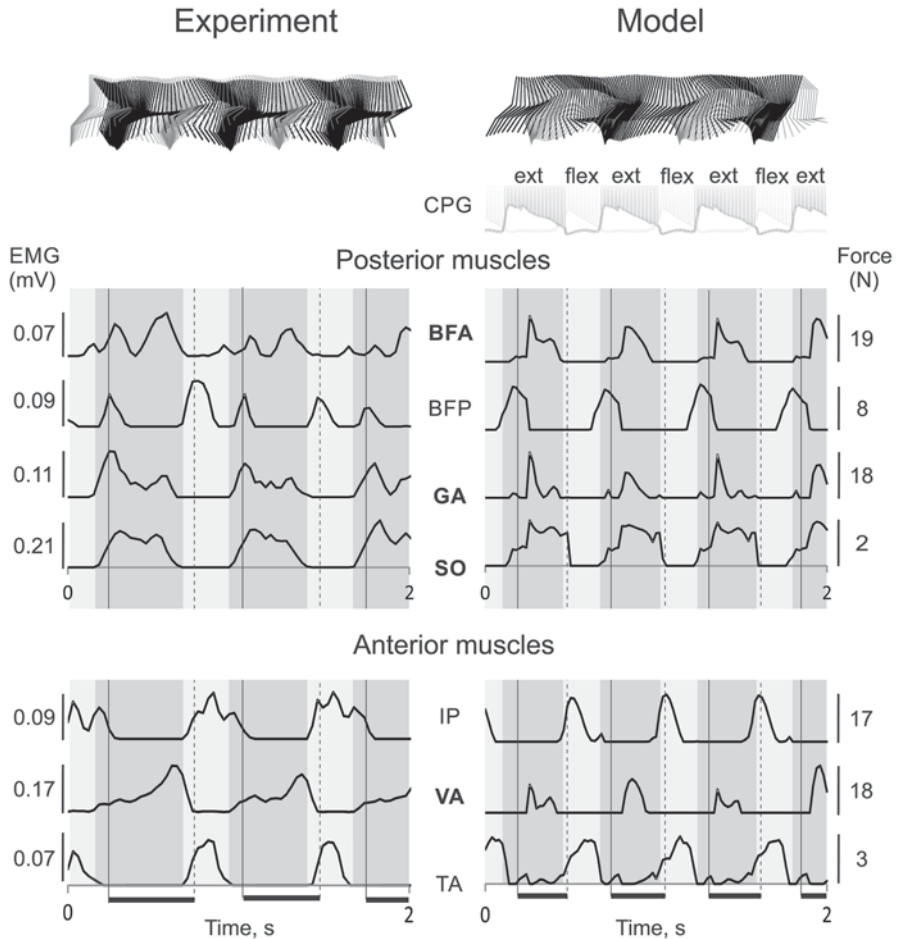


Fig. 12.7 Experimental low-pass filtered EMG patterns of hindlimb muscles during walking (mean cycle duration 0.800 s; *left* panels) and patterns of muscle forces computed in computer simulations (mean cycle duration 0.500, s; *right* panels). For muscle abbreviations see Fig. 12.4; abbreviations of extensor muscles are indicated by bold font. *Top* panels show stick-diagrams of *left* (gray lines) and *right* (black lines) hindlimbs during recorded and simulated walking. Second panel demonstrates bursting activity of the flexor (light lines) and extensor (darker lines) half-centers of the CPG. Next panels show experimental low-pass filtered EMG (*left*) and simulated force patterns (*right*) of selected posterior muscles. The bottom panels demonstrate experimental low-pass filtered EMG (*left*) and simulated force patterns (*right*) of selected anterior muscles. One-joint hindlimb extensors (BFA, GA, SO, VA) are active during extensor phases of CPG activity (dark gray rectangles), while one-joint flexors (IP, TA) are active during flexor phases of CPG activity (light gray rectangles); two-joint BFP demonstrates two bursts of EMG activity in the cycle—at the swing-stance and stance-swing transitions, however simulations show only one period of BFP force production at the swing-stance transitions. Horizontal black bars at bottom indicate stance phases

Computer simulations of cat paw-shakes demonstrated that posterior muscles (BFA, BFP, GA and SO, Fig. 12.4) produced peak muscle forces in phase with the extensor half-center of the CPG, whereas the anterior muscles (IP, VA and TA) produced peak forces during the flexor phase (Fig. 12.6, right panel). Note that VA, one-joint knee extensor, produced force when it did not receive excitatory input from the CPG, while it did not produce force during most of the extensor phase in which it received excitation from the extensor half-center. The low-pass filtered EMG patterns were qualitatively similar to the simulated muscle force patterns except TA appears to generate EMG activity bursts in both phases (Fig. 12.6, left panel).

12.3.3.2 Walking

In order for the model to generate walking-like patterns of muscle activity and hindlimb kinematics, relatively few changes in the reflex pathways were made apart from decreasing rhythm of the HCO from 10 to 2 Hz. The changes included the decrease in gain of Ia afferent feedback from all muscles (Table 12.2) and the introduction of a force-dependent excitation from SO to the CPG extensor half-center and extensor motoneurons during the extensor phase (Table 12.3). The latter change made the extensor phase duration longer than the flexor phase even when the hindlimbs were elevated above the ground and there was no contact of the paw with the ground (air stepping).

Neuromechanical simulations of walking produced hindlimb kinematics and muscle force patterns that were qualitatively similar to those recorded in a representative cat (Fig. 12.7). Specifically, extensor muscles BFA, VA, GA and SO produced force during the extensor (stance) phase of walking, whereas flexors IP and TA produced force during the flexor (swing) phase. Simulations generated force of a two-joint BFP muscle during the swing-stance transitions, although this muscle normally produces two activity bursts at the swing-stance and stance-swing phase transitions (see Chap. 5 by Shevtsova et al. 2015 and Fig. 12.7).

Although the mechanisms underlying the formation of different muscle synergies during paw-shake and walking are not clear and require additional studies, the preliminary computer simulations of paw-shake responses suggested that the knee extensor VA activity burst during the “wrong” flexor phase of the HCO may be caused by Ia length and stretch velocity sensitive afferents from fast elongating VA during this phase (Klishko et al. 2011, 2012). A similar mechanism might explain the absence of EMG burst of VA during the extensor phase of the HCO; although VA motoneuron receives excitation from the extensor half-center during this phase, the reciprocal inhibition via the Ia-inhibitory interneurons (Fig. 12.5) might overcome the CPG excitatory input due to high velocity of stretch of knee flexors, i.e. VA antagonists (BFP, GA and PL) and the corresponding high activity of their Ia afferents (Prochazka et al. 1989).

12.4 Possible Mechanisms of Bistability in the Multifunctional Half-Center Generator

To survive in nature animals should be able to exhibit a large and diverse repertoire of basic behaviors. The rhythmic behaviors like walking, swimming, breathing, etc. are controlled by specialized neuronal circuits, central pattern generators (CPGs). Combining the circuits for different behaviors could make the nervous system more energetically efficient, thus increasing survival chances. There is a great deal of evidence that groups of interneurons can participate in the control of multiple behaviors (Berkowitz et al. 2010). This consideration leads to the concept of multifunctional CPGs. The behavior produced by a multifunctional CPG would be dependent on context and sensory information. Sensory neurons can affect rhythmic activity by directly exciting/inhibiting the CPG neurons. They could also recruit additional neurons to participate in the rhythm suppression of a subset of neurons in such a way as to bias the circuit towards one pattern. The presence of neuromodulators, which is often context dependent, can reconfigure the output of the CPG by changing the electrical properties of neurons and synapses (Hooper and Moulins 1989; Marder et al. 1997; Doi and Ramirez 2008). It is also possible that multiple behaviors could be controlled by a single, multistable CPG. This CPG would be capable of producing multiple behaviors only requiring a single transient input (central or from sensory feedback) to switch between patterns. Our model is a multistable CPG that can produce two different patterns of activity (Fig. 12.2).

There is a large amount of evidence for the existence of multifunctional neurons that participate in more than one motor rhythm (Soffe 1993; Jing and Weiss 2001; Berkowitz 2010). Experiments in cats where a scratching rhythm slowly changed into a walking rhythm provided strong early evidence for overlap in neurons controlling multiple behaviors (Berkinblit et al. 1978), however see (Frigon and Gosard 2010). Much of the best evidence for multifunctional neurons in vertebrates comes from the study of turtles. All spinal interneurons active during one type of scratching in the turtle are also active during other types of scratching, although firing rates vary. There is less overlap for other behaviors that involve the legs, such as swimming and leg withdrawal, but overlap still exists (Berkowitz 2002, 2010). Simultaneous stimulations evoking different motor behaviors and modeling have also demonstrated that there must be either overlap or strong interactions between scratching and swimming CPGs (Hao et al. 2011). In these examples, the exact mechanism determining which pattern the interneurons will produce is not known, although it is likely that sensory information/receptive fields play a role.

Xenopus tadpoles also display two rhythmic behaviors (fast and slow) that appear to originate from a multifunctional CPG: struggling and swimming (2–10 Hz bursting and 10–25 Hz spiking, respectively; speed of oscillation varies across length of the body). These rhythms, and the transition between them, share many features with the behaviors we have modeled. The struggling rhythm occurs when pressure is applied to a tadpole's body (such as being grasped by a predator). This rhythm can also be evoked with repetitive electrical stimulation of the skin sensory

pathway. The swimming rhythm can be evoked with a single stimulation of the same sensory neurons and can persist for a long time. Swimming will occur immediately upon release of pressure or stimulation that causes struggling, and usually begins at a high speed and slows, either to a stop or to a steady velocity. 76% of the motoneurons and 68% of the premotor interneurons involved in struggling are also active during swimming. The additional neurons active during struggling are all of the same classes as those active during swimming (Soffe 1993). The input from the sensory neurons (transient vs. continual) appears to determine which rhythm will be evoked (Soffe 1997). Studies of the transition from struggling to escape swimming revealed that the transition could be gradual under certain conditions (Green and Soffe 1996). Larval zebrafish display similar struggling and swimming behaviors with overlap in neuronal activation. However, in zebrafish, separate classes of inhibitory interneurons are recruited as well (Liao and Fetcho 2008).

Similar to tadpoles, leeches also display two patterns, swimming and crawling, generated by a multifunctional CPG. 93% of the neurons active during swimming are active during crawling, which represent about half of the total neurons involved in crawling. Neurons have been identified that can perturb one or both rhythms if stimulated (Briggman and Kristan 2006). Unlike tadpole struggling and swimming, the presence of neuromodulation plays a role in determining which rhythm these cells produce; application of serotonin will elicit fictive swimming behavior, whereas dopamine will stop swimming and produce crawling (Crisp and Mesce 2004). It is known that serotonin modulates several voltage-dependent currents, including the persistent sodium current (Angstadt and Friesen 1993). In this case, multifunctionality requires the presence of a neuromodulator, at least one of which, dopamine, has been shown to come from higher level inputs (Crisp and Mesce 2004).

Unlike the previous examples, multistability as a mechanism for multifunctional CPGs means that sustained input is not necessary to produce multiple behaviors. Transient sensory input can produce stable changes in network activity. Multistability of circuits and single neurons present a basic feature for mechanisms underlying multifunctional CPGs. Multistability in single neurons has been described in a variety of neurons. Bistability between spiking and silence has been seen in neurons and in models (Jalife and Antzelevitch 1979; Hahn and Durand 2001; Paydarfar et al. 2006; Malashchenko et al. 2011), as well as bistability between spiking and silence (Fuentealba et al. 2004), bursting and spiking (Cymbalyuk et al. 2002; Shilnikov et al. 2005; Fröhlich and Bazhenov 2006), multiple bursting regimes (Butera 1998) and multiple spiking regimes (Egorov et al. 2002; Cymbalyuk and Shilnikov 2005). Switching between silence and spiking in motoneurons has been ascribed to the activation of an L-type calcium channel in the dendrites (Carlin et al. 2000).

Networks of neurons, like CPGs, can display multistability as well, either through multiple modes of firing (silent, spiking, bursting), or through different phase relationships. Network can have multistability without its component neurons being multistable (Bose et al. 2001). In our model we consider a classical paradigm of half-center oscillator (Rybak et al. 2006). This is a common motif in CPGs for producing alternating activity. Multistability in networks can arise through the

dynamics of intrinsic or synaptic currents as opposed to the presence or absence of external input. Our HCO model is multifunctional due to the multistability arising from the dynamics of the two neurons' slow intrinsic currents. With the exact same parameters, multiple rhythms coexist, all of which are stable and will persist indefinitely if left undisturbed. Similar models have been made that display multistability through different mechanisms. Synaptic dynamics in a network can result in multistability. The presence of short term synaptic depression can lead to bistability between two modes: one with a weak synapse and one with a strong synapse. Synaptic depression is both voltage dependent and slow. Synaptic conductance will decrease over the course of consecutive action potentials and recover during silence. Thus, changes in synaptic conductance are similar in mechanism and effect to the changes in I_{CaS} conductance in our model. A two neuron model with depressing synapses can also produce a fast and slow rhythm with the ability to switch back and forth between rhythms with pulses of injected current (Manor and Nadim 2001). Changes in synaptic current are part of the multistability of our model, however, these changes are a result of changes in intrinsic currents (I_{CaS} and I_{NaS}), not their cause. Multistability arising from synaptic dynamics does not depend on intrinsic currents (Bose et al. 2001). The time constant of inhibition can also impart bistability onto a network (Bose and Kunec 2001). Network multistability in terms of the burst phase between four neurons has also been modeled (Chuan et al. 2004).

12.5 Future Studies

12.5.1 Predictions

Based on our findings, it is possible to make several predictions about paw-shaking and walking in cats. In the future, these predictions of the neuromechanical model can be tested. A rapid transition to paw-shaking requires an optimally timed pulse of conductance. This is supported by observations that paw-shaking is always initiated during swing phase of walking (Carter and Smith 1986). It is also necessary for the stimulus to last on the order of the time constant of inactivation for I_{CaS} , which translates to close to the duration of one burst. In the model, at the end of the stimulus pulse, paw-shaking will be slower than normal, then speed up as it approaches its steady state period (usually the difference in period of about 40–30 ms). This is in conflict with data seen in actual cats, which show that paw-shaking generally increases in period from the first to last burst (Smith et al. 1985; Koshland and Smith 1989). This discrepancy could be accounted for by the presence of additional currents or neurons in the cat or by differences in the voltage dependence of inactivation for I_{CaS} .

In terms of the transition back to walking from paw-shaking, the model predicts there will be an asymmetry to the bursts between the two half-centers of the HCO for the first 2–3 cycles post inhibition, which could manifest as a slight discoordination

between muscles/legs immediately after paw-shaking. Although, as with the initial slowness of the paw-shaking rhythm, it is possible that the presence of additional neurons would help stabilize the rhythm faster than two neurons alone could.

12.5.2 *Pharmacological Manipulations*

Paw-shaking and walking could be considered a more excited state and more inhibited state, respectively. Any change in excitation or inhibition will affect both rhythms. We could predict that a brief blockade of the inhibitory synaptic interaction would cause a switch to paw-shaking at about the same speed as excitatory stimulation, and weakening of the synapse would promote paw-shaking. In contrast, strengthening the synapse could abolish the paw-shaking rhythm or make it much more difficult to elicit. Paw-shaking in adult chronic spinalized cats can be eliminated by application of noradrenergic agonist clonidine, which will also increase the period of walking (Barbeau et al. 1987). Experiments in cats show norepinephrine inhibits 43% of interneurons in the ventral horn of the spinal cord, excites 6% and has no effect on the rest (Jordan et al. 1977). Application of NMDA increases expression of paw-shaking, likely by exciting sensory neurons (Chau et al. 2002). Both of these results are in line with our model.

The above predictions could be investigated in details by evoking paw-shake responses in different phases of the walking cycle with different duration of the stimulus.

Acknowledgements This work was supported in part by NSF grant PHY-0750456 to GC, NSF grant IOS 1120291 to DHE, and NIH grants EB012855 and HD032571 and the Center for Human Movement Studies to BIP. The authors would like to thank Dr. David Cofer for his help with developing an earlier version of the cat hindlimb model in AnimatLab.

References

- Angstadt JD, Friesen WO (1993) Modulation of swimming behavior in the medicinal leech. *J Comp Physiol A* 172:235–248
- Barbeau H, Julien C, Rossignol S (1987) The effects of clonidine and yohimbine on locomotion and cutaneous reflexes in the adult chronic spinal cat. *Brain Res* 437:83–96
- Berkinblit MB, Deliagina TG, Feldman AG, Gelfand IM, Orlovsky GN (1978) Generation of scratching. II. Nonregular regimes of generation. *J Neurophysiol* 41:1058–1069
- Berkowitz A (2002) Both shared and specialized spinal circuitry for scratching and swimming in turtles. *J Comp Physiol A* 188:225–234
- Berkowitz A (2010) Multifunctional and specialized spinal interneurons for turtle limb movements. *Ann N Y Acad Sci* 1198:119–132
- Berkowitz A, Roberts A, Soffe SR (2010) Roles for multifunctional and specialized spinal interneurons during motor pattern generation in tadpoles, zebrafish larvae, and turtles. *Front Behav Neurosci* 4:1–18

- Bose A, Kunec S (2001) Synchrony and frequency regulation by synaptic delay in networks of self-inhibiting neurons. *Neurocomputing* 38–40:505–513
- Bose A, Manor Y, Nadim F (2001) Bistable oscillations arising from synaptic depression. *SIAM J Appl Math* 62:706–727
- Boyd SK, Ronsky JL (1998) Instantaneous moment arm determination of the cat knee. *J Biomech* 31:279–283
- Briggman KL, Kristan WB (2006) Imaging dedicated and multifunctional neural circuits generating distinct behaviors. *J Neurosci* 26:10925–10933
- Briggman KL, Kristan WB (2008) Multifunctional pattern-generating circuits. *Annu Rev Neurosci* 31:271–294
- Brown TG (1911) The intrinsic factors in the act of progression in the mammal. *Proc R Soc Lond Series B, Contain Pap Biol Character* 84:308–319
- Butera RJ (1998) Multirhythmic bursting. *Chaos* 8:274–284
- Canavier CC, Baxter DA, Clark JW, Byrne JH (1993) Nonlinear dynamics in a model neuron provide a novel mechanism for transient synaptic inputs to produce long-term alterations of postsynaptic activity. *J Neurophysiol* 69:2252–2257
- Carlin KP, Jones KE, Jiang Z, Jordan LM, Brownstone RM (2000) Dendritic L-type calcium currents in mouse spinal motoneurons: implications for bistability. *Eur J Neurosci* 12:1635–1646
- Carter MC, Smith JL (1986) Simultaneous control of two rhythmical behaviors. II. Hindlimb walking with paw-shake response in spinal cat. *J Neurophysiol* 56:184–195
- Chau C, Giroux N, Barbeau H, Jordan L, Rossignol S (2002) Effects of intrathecal glutamatergic drugs on locomotion I. NMDA in short-term spinal cats. *J Neurophysiol* 88:3032–3045
- Chuan L, Clark JW, Canavier CC, Baxter DA, Byrne JH (2004) Multimodal behavior in a four neuron ring circuit: mode switching. *IEEE Trans Biomed Eng* 51:205–218
- Cofer D, Cymbalyuk G, Reid J, Zhu Y, Heitler WJ, Edwards DH (2010) AnimatLab: a 3D graphics environment for neuromechanical simulations. *J Neurosci Methods* 187:280–288
- Conway BA, Hultborn H, Kiehn O (1987) Proprioceptive input resets central locomotor rhythm in the spinal cat. *Exp Brain Res* 68:643–656
- Crisp KM, Mesce KA (2004) A cephalic projection neuron involved in locomotion is dye coupled to the dopaminergic neural network in the medicinal leech. *J Exp Biol* 207:4535–4542
- Cymbalyuk G, Shilnikov A (2005) Coexistence of tonic spiking oscillations in a leech neuron model. *J Comput Neurosci* 18:255–263
- Cymbalyuk GS, Gaudry Q, Masino MA, Calabrese RL (2002) Bursting in leech heart interneurons: cell-autonomous and network-based mechanisms. *J Neurosci* 22:10580–10592
- Doi A, Ramirez J-M (2008) Neuromodulation and the orchestration of the respiratory rhythm. *Respir Physiol Neurobiol* 164:96–104
- Eccles JC, Eccles RM, Lundberg A (1957) Synaptic actions on motoneurons caused by impulses in golgi tendon organ afferents. *J Physiol* 138:227–252
- Egorov AV, Hamam BN, Fransén E, Hasselmo ME, Alonso AA (2002) Graded persistent activity in entorhinal cortex neurons. *Nature* 420:173–178
- Feldman AG, Orlovsky GN (1975) Activity of interneurons mediating reciprocal Ia inhibition during locomotion. *Brain Res* 84:181–194
- Friesen OW (1994) Reciprocal inhibition: a mechanism underlying oscillatory animal movements. *Neurosci Biobehav Rev* 18:547–553
- Frigon A, Gossard JP (2010) Evidence for specialized rhythm-generating mechanisms in the adult mammalian spinal cord. *J Neurosci* 30:7061–7071
- Fröhlich F, Bazhenov M (2006) Coexistence of tonic firing and bursting in cortical neurons. *Phys Rev E* 74:031922
- Fuentealba P, Timofeev I, Bazhenov M, Sejnowski TJ, Steriade M (2004) Membrane bistability in thalamic reticular neurons during spindle oscillations. *J Neurophysiol* 93:294–304
- Geertsen SS, Stecina K, Meehan CF, Nielsen JB, Hultborn H (2011) Reciprocal Ia inhibition contributes to motoneuronal hyperpolarisation during the inactive phase of locomotion and scratching in the cat. *J Physiol* 589:119–134

- Getting PA (1989) Emerging principles governing the operation of neural networks. *Annu Rev Neurosci* 12:185–204
- Goslow GE Jr, Reinking RM, Stuart DG (1973) The cat step cycle: hind limb joint angles and muscle lengths during unrestrained locomotion. *J Morphol* 141:1–41
- Green CS, Soffe SR (1996) Transitions between two different motor patterns in *Xenopus* embryos. *J Comp Physiol A* 178:279–291
- Gregor RJ, Smith DW, Prilutsky BI (2006) Mechanics of slope walking in the cat: quantification of muscle load, length change, and ankle extensor EMG patterns. *J Neurophysiol* 95:1397–1409
- Grillner S (1981) Control of locomotion in bipeds, tetrapods, and fish. In: Brooks V (ed) *Handbook of physiology*. Section I. The nervous system, vol II, pp 1179–1236. American Physiological Society, Bethesda
- Grillner S (2006) Biological pattern generation: the cellular and computational logic of networks in motion. *Neuron* 52:751–766
- Guttman R, Lewis S, Rinzel J (1980) Control of repetitive firing in squid axon membrane as a model for a neurooscillator. *J Physiol* 305:377–395
- Hahn P, Durand D (2001) Bistability dynamics in simulations of neural activity in high-extracellular-potassium conditions. *J Comput Neurosci* 11:5–18
- Hao Z-Z, Spardy LE, Nguyen EBL, Rubin JE, Berkowitz A (2011) Strong interactions between spinal cord networks for locomotion and scratching. *J Neurophysiol* 106:1766–1781
- Hiebert GW, Whelan PJ, Prochazka A, Pearson KG (1996) Contribution of hind limb flexor muscle afferents to the timing of phase transitions in the cat step cycle. *J Neurophysiol* 75:1126–1137
- Hodgkin AL, Huxley AF (1952) A quantitative description of membrane current and its application to conduction and excitation in nerve. *J Physiol* 117:500–544
- Hooper S, Moulins M (1989) Switching of a neuron from one network to another by sensory-induced changes in membrane properties. *Science* 244:1587–1589
- Hounsgaard J, Kiehn O (1989) Serotonin-induced bistability of turtle motoneurons caused by a nifedipine-sensitive calcium plateau potential. *J Physiol* 414:265–282
- Hounsgaard J, Hultborn H, Jespersen B, Kiehn O (1984) Intrinsic membrane properties causing a bistable behaviour of α -motoneurons. *Exp Brain Res* 55:391–394
- Hoy MG, Zernicke RF (1985) Modulation of limb dynamics in the swing phase of locomotion. *J Biomech* 18:49–60
- Hughes SW, Cope DW, Tóth TI, Williams SR, Crunelli V (1999) All thalamocortical neurones possess a T-type Ca^{2+} ‘window’ current that enables the expression of bistability-mediated activities. *J Physiol* 517:805–815
- Jalife J, Antzelevitch C (1979) Phase resetting and annihilation of pacemaker activity in cardiac tissue. *Science* 206:695–697
- Jing J, Weiss KR (2001) Neural mechanisms of motor program switching in Aplysia. *J Neurosci* 21:7349–7362
- Jordan LM, McCrea DA, Steeves JD, Menzies JE (1977) Noradrenergic synapses and effects of noradrenaline on interneurons in the ventral horn of the cat spinal cord. *Can J Physiol Pharmacol* 55:399–412
- Klishko AN, Cofer D, Cymbalyuk G, Gregor RJ, Edwards DH, Prilutsky BI (2011) Contributions of proprioceptive feedback and CPG to coordination of two-joint muscles during a paw shake response: a computer simulation study. Program No. 920.10. Society for Neuroscience. Society for Neuroscience, 2011. Online, Washington, DC
- Klishko AN, Cofer D, Cymbalyuk G, Edwards DH, Prilutsky BI (2012) Paw-shake response and locomotion: can one CPG generate two different rhythmic behaviors? Twenty first annual computational neuroscience meeting: CNS 2012, vol 13(Suppl 1), p 70, BioMed Central Ltd., Atlanta/Decatur, GA, USA
- Koshland GF, Smith JL (1989) Mutable and immutable features of paw-shake responses after hindlimb deafferentation in the cat. *J Neurophysiol* 62:162–173
- Kriellaars DJ, Brownstone RM, Noga BR, Jordan LM (1994) Mechanical entrainment of fictive locomotion in the decerebrate cat. *J Neurophysiol* 71:2074–2086

- Laporte Y, Lloyd DP (1952) Nature and significance of the reflex connections established by large afferent fibers of muscular origin. *Am J Physiol* 169:609–621
- Lechner HA, Baxter DA, Clark JW, Byrne JH (1996) Bistability and its regulation by serotonin in the endogenously bursting neuron R15 in *Aplysia*. *J Neurophysiol* 75:957–962
- Liao JC, Fetcho JR (2008) Shared versus specialized glycinergic spinal interneurons in axial motor circuits of larval zebrafish. *J Neurosci* 28:12982–12992
- Lieske SP, Thoby-Brisson M, Telgkamp P, Ramirez JM (2000) Reconfiguration of the neural network controlling multiple breathing patterns: eupnea, sighs and gasps. *Nat Neurosci* 3:600
- Lockery S, Kristan W (1990) Distributed processing of sensory information in the leech. II. Identification of interneurons contributing to the local bending reflex. *J Neurosci* 10:1816–1829
- MacFadden LN, Brown NA (2007) Biarticular hip extensor and knee flexor muscle moment arms of the feline hindlimb. *J Biomech* 40:3448–3457
- MacFadden LN, Brown NA (2010) The influence of modeling separate neuromuscular compartments on the force and moment generating capacities of muscles of the feline hindlimb. *J Biomech Eng* 132:081003
- Malashchenko T, Shilnikov A, Cymbalyuk G (2011) Bistability of bursting and silence regimes in a model of a leech heart interneuron. *Phys Rev E* 84:041910
- Manor Y, Nadim F (2001) Synaptic depression mediates bistability in neuronal networks with recurrent inhibitory connectivity. *J Neurosci* 21:9460–9470
- Marder E, Bucher D (2001) Central pattern generators and the control of rhythmic movements. *Curr Biol* 11:R986–R996
- Marder E, Calabrese RL (1996) Principles of rhythmic motor pattern generation. *Physiol Rev* 76:687–717
- Marder E, Jorge-Rivera JC, Kilman V, Weimann JM (1997) Peptidergic modulation of synaptic transmission in a rhythmic motor system. *Adv Organ Biol* 2:213–233 (Elsevier, Bittar EE (ed))
- Markin SN, Lemay MA, Prilutsky BI, Rybak IA (2012) Motoneuronal and muscle synergies involved in cat hindlimb control during fictive and real locomotion: a comparison study. *J Neurophysiol* 107:2057–2071
- McCrea DA (2001) Spinal circuitry of sensorimotor control of locomotion. *J Physiol* 533:41–50
- McCrea DA, Rybak IA (2008) Organization of mammalian locomotor rhythm and pattern generation. *Brain Res Rev* 57:134–146
- McVea DA, Donelan JM, Tachibana A, Pearson KG (2005) A role for hip position in initiating the swing-to-stance transition in walking cats. *J Neurophysiol* 94:3497–3508
- Mehta R, Prilutsky BI (2014) Task-dependent inhibition of slow-twitch soleus and excitation of fast-twitch gastrocnemius do not require high movement speed and velocity-dependent sensory feedback. *Front Physiol* 5:410
- Newman JP, Butera RJ (2010) Mechanism, dynamics, and biological existence of multistability in a large class of bursting neurons. *Chaos* 20:023118
- Nichols TR (1999) Receptor mechanisms underlying heterogenic reflexes among the triceps surae muscles of the cat. *J Neurophysiol* 81:467–478
- Nichols TR, Bunderson N, Lyle M (2015) Neural regulation of limb mechanics: insights from the organization of proprioceptive circuits. In: Prilutsky BI, Edwards DH Jr (eds) *Neuromechanical modeling of posture and locomotion*. Springer, New York (in press)
- Paydarfar D, Forger DB, Clay JR (2006) Noisy inputs and the induction of on–off switching behavior in a neuronal pacemaker. *J Neurophysiol* 96:3338–3348
- Pearson KG (2008) Role of sensory feedback in the control of stance duration in walking cats. *Brain Res Rev* 57:222–227
- Pearson KG, Rossignol S (1991) Fictive motor patterns in chronic spinal cats. *J Neurophysiol* 66:1874–1887
- Popescu IR, Frost WN (2002) Highly dissimilar behaviors mediated by a multifunctional network in the marine mollusk *Tritonia diomedea*. *J Neurosci* 22:1985–1993
- Pratt CA, Chanaud CM, Loeb GE (1991) Functionally complex muscles of the cat hindlimb. IV. Intramuscular distribution of movement command signals and cutaneous reflexes in broad, bifunctional thigh muscles. *Exp Brain Res* 85:281–299

- Prilutsky BI, Gregor RJ, Nichols TR (2004) Coordination of cat ankle extensors during the paw-shake before and after self-reinnervation of medial and lateral gastrocnemius muscles. Program No. 69.12. In 2004 neuroscience meeting planner (ed), Society for Neuroscience. Online, San Diego, CA
- Prilutsky B, Klishko AN, Farrell B, Harley L, Philips G, Bottasso CL (2009) Movement coordination in skilled tasks: insights from optimization. In Shinohara M (ed) *Advances in neuromuscular physiology of motor skills and muscle fatigue*, pp 139–171. Research Signpost, Kerala
- Prilutsky BI, Maas H, Bulgakova M, Hodson-Tole EF, Gregor RJ (2011) Short-term motor compensations to denervation of feline soleus and lateral gastrocnemius result in preservation of ankle mechanical output during locomotion. *Cells Tissues Organs* 193:310–324
- Prochazka A, Hulliger M, Trend P, Llewellyn M, Durmuller N (1989) Muscle afferent contribution to control of paw shakes in normal cats. *J Neurophysiol* 61:550–562
- Rinzel J (1978) On repetitive activity in nerve. *Fed Proc* 37:2793–2802
- Ritzmann RE, Tobias ML, Fournier CR (1980) Flight activity initiated via giant interneurons of the cockroach: evidence for bifunctional trigger interneurons. *Science* 210:443–445
- Rossignol S (2006) Plasticity of connections underlying locomotor recovery after central and/or peripheral lesions in the adult mammals. *Philos Trans R Soc Lond B Biol Sci* 361:1647–1671
- Rybak IA, Shevtsova NA, Lafreniere-Roula M, McCrea DA (2006) Modelling spinal circuitry involved in locomotor pattern generation: insights from deletions during fictive locomotion. *J Physiol* 577:617–639
- Shevtsova NA, Hamade K, Chakrabarty S, Markin SN, Prilutsky BI, Rybak IA (2015) Modeling the organization of spinal neural circuits controlling two-joint muscles. In: Prilutsky BI, Edwards DH Jr (eds) *Neuromechanical modeling of posture and locomotion*, vol 12. Springer, New York (in press)
- Shilnikov A, Calabrese RL, Cymbalyuk G (2005) Mechanism of bistability: tonic spiking and bursting in a neuron model. *Phys Rev E* 71:056214
- Smith JL, Zernicke RF (1987) Predictions for neural control based on limb dynamics. *Trends Neurosci* 10:123–128
- Smith JL, Hoy MG, Koshland GF, Phillips DM, Zernicke RF (1985) Intralimb coordination of the paw-shake response: a novel mixed synergy. *J Neurophysiol* 54:1271–1281
- Soffe S (1993) Two distinct rhythmic motor patterns are driven by common premotor and motor neurons in a simple vertebrate spinal cord. *J Neurosci* 13:4456–4469
- Soffe SR (1997) The pattern of sensory discharge can determine the motor response in young *Xenopus* tadpoles. *J Comp Physiol A* 180:711–715
- Syed NI, Winlow W (1991) Respiratory behavior in the pond snail *Lymnaea stagnalis*. *J Comp Physiol A* 169:557–568
- Turrigiano GG, Marder E, Abbott LF (1996) Cellular short-term memory from a slow potassium conductance. *J Neurophysiol* 75:963–966
- Vogels TP, Rajan K, Abbott LF (2005) Neural network dynamics. *Annu Rev Neurosci* 28:357–376
- Wang X-J, Rinzel J (1992) Alternating and synchronous rhythms in reciprocally inhibitory model neurons. *Neural Comput* 4:84–97